

---

# The Effects of Aspect Ratio on Global Persistence Length and Backfolding for Worm-Like Polymers Confined to Rectangular Nanochannels

---

MICHAEL J QUEVILLON

Submitted under the supervision of DR. KEVIN D DORFMAN to the University Honors Program at the University of Minnesota-Twin Cities in partial fulfillment of the requirements for the degree of Bachelor of Chemical Engineering, *cum laude*.

June 15, 2015

# Contents

<b>Abstract</b>	<b>2</b>
<b>1 Introduction</b>	<b>3</b>
<b>2 Methods and Models</b>	<b>4</b>
2.1 Ideal Random Walks . . . . .	4
2.2 Self-Avoiding Walks . . . . .	8
2.3 Worm-Like Chain Model . . . . .	9
2.4 Discretized Worm-Like Chain Model . . . . .	10
2.5 Pruned-Enriched Rosenbluth Method . . . . .	12
<b>3 Theories</b>	<b>17</b>
3.1 Global Persistence Length . . . . .	17
3.2 Odijk Scaling Theory . . . . .	20
<b>4 Simulation Results</b>	<b>23</b>
4.1 Ideal Chains . . . . .	23
4.2 Real Chains . . . . .	25
<b>5 Summary &amp; Future Work</b>	<b>27</b>
<b>6 Acknowledgements</b>	<b>29</b>
<b>References</b>	<b>30</b>

## Abstract

In pursuit of a better understanding of the properties and behaviors of worm-like polymer chains, we present data generated from large-scale simulations of a discretized worm-like chain in confinement employing the pruned-enriched Rosenbluth method (PERM). In this publication, we focus on confinement channels of rectangular cross-section. We find that the simulations support two distinct Odijk regimes for these worm-like chains: the classic Odijk regime made up of deflection segments oriented approximately in the same direction, and a second regime where the chain folds up on itself within the channel to create backfolds, or hairpin turns. The rectangular channel results are presented in a similar fashion to the previous studies of their square counterparts.

This backfolded regime is posited as an explanation for the transition between classic regimes, which is where many DNA confinement experiments fit in, due to DNA's stiff nature. The crossover between the classic and backfolded Odijk regimes is also shown in agreement to theory. The theory also predicts a power law between chain extension and Odijk's scaling parameter for rectangular channels,  $\xi_3$ , which is corroborated with data presented here. While the backfolded regime covers only a narrow range of channel sizes, the definition of  $\xi_3$  allows for finer differentiation between regimes.

# 1 Introduction

Our motivation for this project stems from discrepancies between experimental results and theory presented in Reisner *et al.*'s formative research<sup>1</sup> for DNA molecules confined to nanochannels. None of the previously-proposed regimes could explain the data. For worm-like chains (detailed in section 2.3) with a persistence length,  $\ell_p$ , and a width,  $w$ , confined to a nanochannel with a square cross-section of width  $D$ , there are two well-studied regimes in the limits of strong confinement and weak confinement. In strong confinement ( $D \ll \ell_p$ ), the classic Odijk regime<sup>2</sup> is apparent. The classic Odijk regime is characterized by deflection segments that zig-zag across the channel and by the tendency of the chain to grow in one direction along the channel. The classic de Gennes regime<sup>3</sup> is characterized by spherical “blobs” of entwined chain length that form within the channel due to weak confinement ( $D > \ell_p^2/w$ ). The region between these two distinct regimes is where our interests lie.

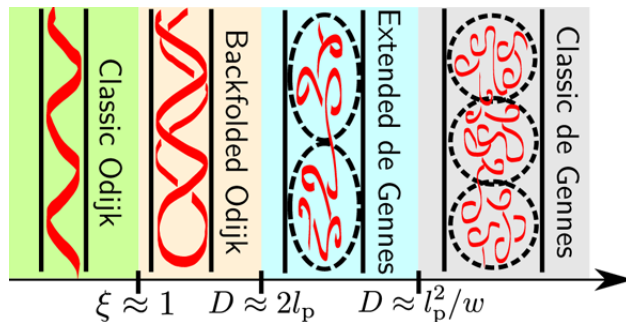


Figure 1: A comparison of regimes for various degrees of confinement compared to channel sizes (larger channels on the right). The classic Odijk regime is shown here with 5 deflection segments. The backfolded Odijk regime is distinguished from its classic counterpart by the existence of hairpin turns called backfolds (one shown at bottom). The characteristic “blobs” are observed in both the classical and extended de Gennes regimes. (Reproduced from reference 4.)

Brochard-Wyart *et al.* present compelling evidence<sup>5</sup> to support an “extended de Gennes” regime, characterized by elongated blobs, but still resembling the classic de Gennes behavior. This regime lessens the gap between strong and weak confinement, but there is still much ground to be covered. More recently, Odijk presented a theory<sup>6</sup> to hopefully connect the regimes for all combinations of persistence length and channel size. In a parallel to the

extended de Gennes regime, Odijk extends the deflection segment model to include backfolding, or hairpin turns, in which the chain reverses its direction in the channel. To measure this long range ( $\geq \ell_p$ ) bending property, a new parameter is introduced: the global persistence length,  $g$  (detailed in section 3.1). This global persistence length should be able to extend into the extended de Gennes regime as  $g$  approaches  $\ell_p$ . A dimensionless parameter,  $\xi$ , incorporates both persistence lengths, the size of the channel and the width of the chain to characterize the backfolding scaling theory.<sup>7</sup>

These regimes have been well-defined for channels with square and circular cross-sections, but rectangular cross-sections may be more useful in the creation of microfluidic devices where, for example, one dimension may be held constant to keep a consistent thickness across devices of varying cross-sectional area. With the backfolding scaling theory for square channels, similar scaling theories were also proposed for rectangular channels.<sup>7</sup> Simulations from our research group have already shown support for the scaling theories in square channels;<sup>4</sup> we now present simulation data in support of Odijk’s backfolding scaling theories for rectangular nanochannels.

## 2 Methods and Models

### 2.1 Ideal Random Walks

There are several algorithms for creating random walk polymers, but the method detailed in this section is a building block for the method of the full simulation (Pruned-Enriched Rosenbluth Method, or PERM). For an ideal polymer chain, each monomer of the polymer chain can be represented by a point in three-dimensional space that has no volume. In addition, the interactions (i.e. van der Waals forces) between particles are ignored. These points are connected so that the order of the monomers is retained. The distance between any two neighboring points is fixed to be the statistical segment length of a given monomer,<sup>8</sup> but since each point has no volume, the distance between any two points that are not neighboring

is not a definitive value. This means two non-neighboring points are allowed to overlap exactly, which differs greatly from any intuitive knowledge of objects in three-dimensions. (Two physical solid objects with cannot intersect each other, in the most common sense.) To obtain a simulated configuration of a polymer chain such as these, the chain is built up one monomer at a time via a random walk.

In an unconfined random walk, the origin of the coordinate system is typically defined as the position of the first monomer. To determine where the second monomer should be placed, a random direction is chosen and the next monomer is placed at a fixed distance from the first monomer. The locus of positions where the next monomer can be placed is a sphere of a fixed radius with the previous monomer at the center. To choose a random direction, we must choose a random point from this sphere. However, it is not sufficient to choose a random pair of polar and azimuthal angles,  $(\theta, \phi)$ , from the spherical coordinate system. This incorrect method gives too many points near the poles of the sphere, causing an unwanted bias in the system, as seen in figure 2. Marsaglia<sup>9</sup> discusses three existing methods of choosing a point from the surface of a sphere and proposes a new method that requires fewer uniform variates (on average) and is faster than any of the other presented methods. Due to its performance and few random numbers, Marsaglia's method is used throughout this discussion to obtain a random direction.

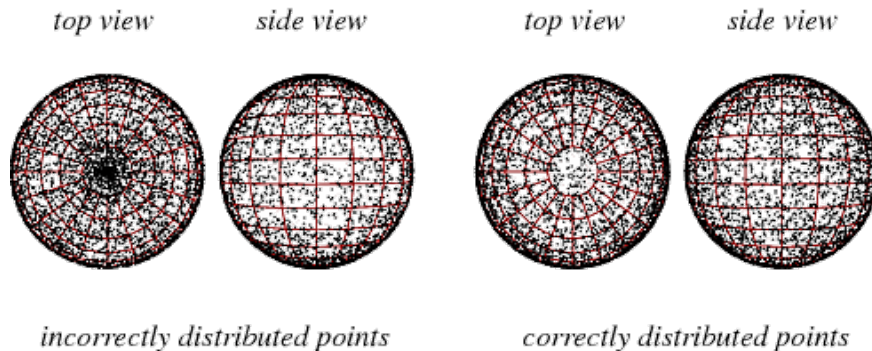


Figure 2: A comparison of spherical point picking distributions. The left sphere shows points chosen from a normal distribution of  $\theta \in [0, 2\pi)$  and  $\phi \in [0, \pi)$ , whereas the right sphere shows the proper spherical distribution. (Reproduced from reference 10.)

The algorithm is as follows: choose two independent uniform distributions,  $V_1$  and  $V_2$ , on

the interval  $(-1, 1)$ . Reject these points if  $V_1^2 + V_2^2 \geq 1$ . Otherwise, the unit vector,  $\langle \tilde{x}, \tilde{y}, \tilde{z} \rangle$ , to the new random point is given by

$$\begin{cases} \tilde{x} &= 2V_1\sqrt{1 - V_1^2 - V_2^2} \\ \tilde{y} &= 2V_2\sqrt{1 - V_1^2 - V_2^2} \\ \tilde{z} &= 1 - 2(V_1^2 + V_2^2). \end{cases} \quad (1)$$

This vector has a length of 1, but can either be used in a dimensionless space such that the distance between monomers is fixed at 1 or scaled to the appropriate length. If the distance between monomers is represented by  $d$ , the vector,  $\langle x, y, z \rangle$ , to the next monomer is given by

$$\begin{cases} x = d\tilde{x} \\ y = d\tilde{y} \\ z = d\tilde{z}. \end{cases} \quad (2)$$

The next monomer is then placed at the end of this vector, and the process is repeated until the desired length of chain is reached.

The placement of a monomer unit is dependent only on its immediate predecessor, not on any other part of the polymer, since the zero-volume monomers have no interactions with their surroundings. When the positions of the monomers along the entire length of the chain have been determined, the random walk algorithm is complete. The resulting set of points that make up this configuration can then be analyzed to obtain properties about this specific chain, such as center of mass, radius of gyration, and extension in any direction. While the exact relation between any two non-neighboring monomers is not known, these configuration-dependent properties can somewhat characterize this polymer. With enough random walks, statistics can be calculated for these properties to reveal scaling relations. One useful relation<sup>8</sup> obtained from this model relates the radius of gyration,  $R_g$ , and the average squared end-to-end distance,  $\langle h^2 \rangle$ , to the number of segments,  $N$ , and the statistical

segment length (or Kuhn length<sup>11</sup>),  $b$ , through

$$R_g^2 = \frac{\langle h^2 \rangle}{6} = \frac{Nb^2}{6}. \quad (3)$$

Since a random walk can go in one direction and take the next step in the opposite direction, the most probable value of the end-to-end distance of an unconfined configuration will be 0. For enough one-dimensional random walks, the distribution of the end-to-end distance is centered at zero and is Gaussian in shape.<sup>8</sup> When moving to the three-dimensional statistics, more trials are required to begin to see a Gaussian distribution in three dimensions. (This is achieved using spherical coordinates and plotting against the radial direction, due to angular symmetry of the random walk.)

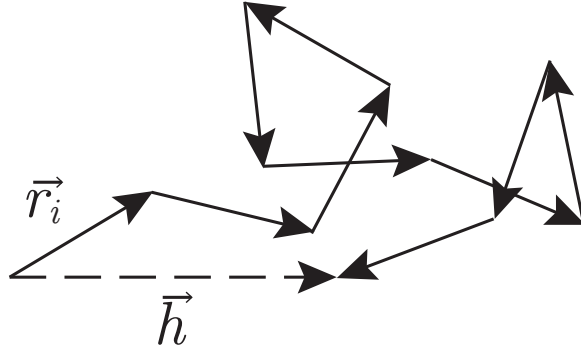


Figure 3: An ideal random walk of length  $N = 10$  in two dimensions.  $\vec{r}_i$  is the vector connecting monomers  $i$  and  $i + 1$ ;  $\vec{h}$  is the end-to-end vector. Since the monomers are zero-volume, the two pairs of crossing segments is allowed.

Due to all of this method's assumptions, it will not produce many real-world applicable results. This is only a first method that is built upon to create sophisticated simulation techniques. Without yet incorporating the interactions between molecules within the polymer chain, the next logical step is to account for the volume that a monomer contains.



## 2.2 Self-Avoiding Walks

In order to determine how a simulated polymer chain will avoid self-intersection, we can use a slightly more advanced model that uses a lattice, where monomers can only be placed at specific sites. Many studies have been performed on self-avoiding walks on various shapes of lattices (i.e. cubic,<sup>12-14</sup> triangular,<sup>15,16</sup> tetrahedral,<sup>17</sup> and face-centered cubic<sup>16</sup>), with cubic being the most common and intuitive, due to its simple representation in the standard Cartesian coordinate system. Self-avoiding walks outside of the field of polymer physics have also been greatly studied by mathematicians (sometimes called a lattice path, in this case) such as Domb,<sup>18</sup> Abbott & Hanson,<sup>19</sup> and Kesten.<sup>20</sup>

When a simulated polymer chain is restricted to a lattice, the monomers can still be represented as zero-volume points (as in the ideal random walk) with a fixed distance between neighboring monomers. In this case, the lattice spacing ensures the fixed distance between monomers. Taking the cubic lattice as an example, there are at most six directions in which the next monomer can be placed (positive and negative directions in each of the  $x$ ,  $y$ , and  $z$  dimensions). This occurs only during the placement of the second monomer. For the third monomer (and its successors), there are fewer than six directions since some directions will cause a self-intersection. The restriction to lattice points means that the only way for two monomers to intersect (or overlap), is by being located at the exact same point on the lattice. Typically, self-avoiding walk algorithms will reject a configuration as soon as two monomers intersect, which is why many walks must be performed to get an adequate number of full-length trials. This effect will be even greater when the chain gets longer, since it will try to coil in on itself, but it is still restricted to be self-avoiding. If it coils into a place where there are no possible choices for the next monomer (and the chain is not the desired length yet), that configuration is ended and either kept as a shorter-than-desired chain or rejected entirely.

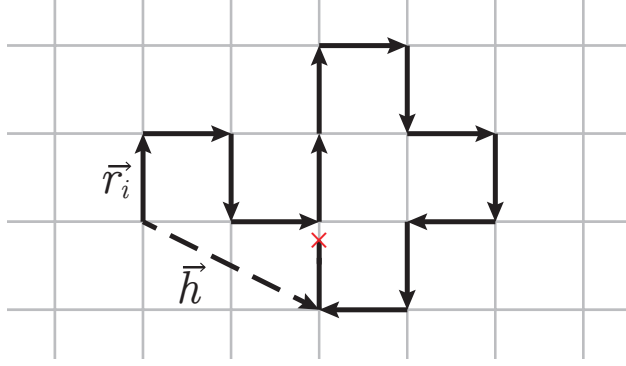


Figure 4: A self-avoiding walk of length  $N = 13$  on a square lattice in two dimensions.  $\vec{r}_i$  is the vector connecting monomers  $i$  and  $i + 1$ ;  $\vec{h}$  is the end-to-end vector. The simulation is ended when the trial 14<sup>th</sup> segment is placed in such a way that would self-intersect, represented as a red  $\times$ . The end-to-end vector is calculated by using the last properly added segment (the 13<sup>th</sup> in this case).

An alternative to rejecting configurations is to keep all walks, regardless of size. This will mean that, for a given data set, there will be much better statistics for the shorter chain lengths, since it is difficult for a self-avoiding random walk to produce a long chain. In order to observe statistics for long chain limits, a “smarter” algorithm must be used, such as the Pruned-Enriched Rosenbluth Method (discussed in section 2.5).

## 2.3 Worm-Like Chain Model

In the aforementioned methods, the placement of one monomer has mostly been affected by the positioning of the previous monomer. In the worm-like chain (WLC) model,<sup>21</sup> the polymer is made up of a continuously flexible rod. The cross-sectional size of the chain is determined by the size and shape of the monomer itself, but does not affect the model’s behavior. (This model is an ideal, zero-volume chain.) The amount that the rod can bend is called the persistence length,  $\ell_p$ , which is characteristic of a polymer. The persistence length is the distance along the polymer before the orientation changes appreciably due to thermal fluctuations.<sup>8</sup> (Bending due to external forces does not factor in to the persistence length.) Defining this persistence length allows the WLC model to limit the amount of bending in the continuous polymer rod. The Kratky-Porod model for worm-like chains<sup>22</sup>

is useful for polymers under extensional forces, but can only be solved for small forces,<sup>23</sup> which can be applicable to polymers in bulk (unconfined). This model is very useful for stiff molecules, such as DNA,<sup>24</sup> but can be difficult to simulate numerically, which can be solved by discretizing the worm into finite segments as in section 2.4.

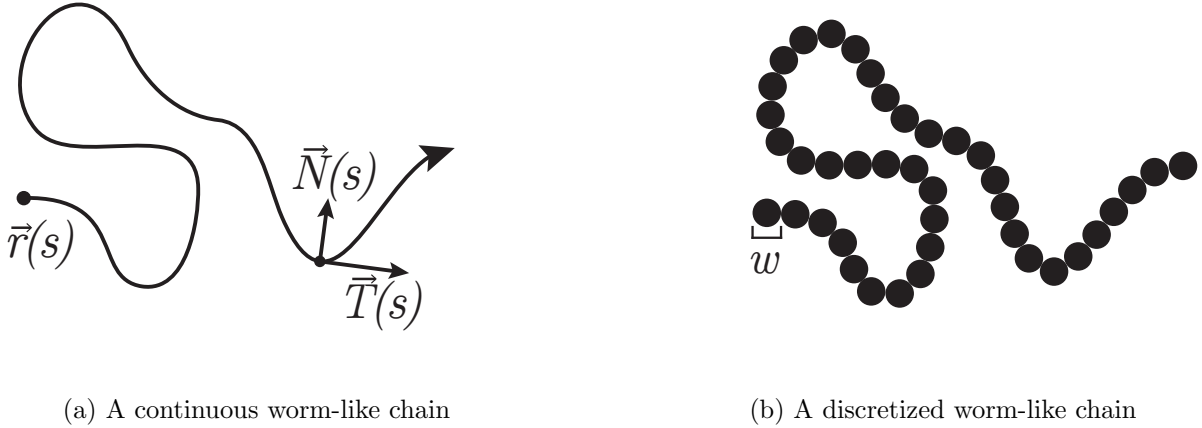


Figure 5: A comparison of the same polymer simulated using a continuous worm-like chain (a) and a discretized worm-like chain (b). Since (a) is a continuous model, it can be represented by a smooth curve,  $\vec{r}(s)$ , parameterized by arclength,  $s$ . The tangent and normal vectors,<sup>25</sup>  $\vec{T}$  and  $\vec{N}$ , are labeled at one point, but have values for the entire length of the chain. Both models have a contour length  $L$ , but (b) is discretized into  $N = L/w$  segments represented by  $N + 1$  beads.

## 2.4 Discretized Worm-Like Chain Model

The final model to be discussed is the discretized worm-like chain (DWLC) model,<sup>26</sup> which is a combination of most of the previously mentioned models. Instead of a continuous length of chain like in the WLC model, the chain is broken into spheres with a diameter equal to the distance between repeat units in a polymer. The DWLC model is able to model, to appreciable accuracy, a continuous WLC, given that the number of discrete segments is high enough. On the other hand, it is also able to reproduce the results from freely-jointed chains (where the angle to the next monomer is unrestricted). This means that, when given the proper parameters, the DWLC model is versatile and accurate at describing a wide variety of polymers.

An interesting category of molecules to simulate is DNA because the single-stranded and double-stranded types differ greatly in their properties. In many cases, the double-stranded DNA is so stiff that it requires the continuous WLC model with high persistence lengths. Single-stranded DNA is not as stiff, and is typically modeled with a discrete model. Tree *et al.* argue<sup>26</sup> for the use of DWLC to properly model both types of DNA, with the caveat that base-pair and stacking interactions are neglected. The interests of this research group lie in microfluidics and the physics of DNA molecules, so the DWLC model is well-suited for our applications. Hence, this model is employed in our simulations, and will be described in more detail below.

In this model, we have  $N + 1$  “beads” (spheres) of diameter  $w$  connected by  $N$  bonds of a fixed length,  $a$ . This gives an overall contour length of

$$L = Na. \quad (4)$$

In order to build a configuration, the potential energies are calculated, and higher-energy configurations are penalized while lower-energy configurations are more preferred. There are several terms that make up the overall potential energy of a chain, but the main contributors are bending energy and excluded volume, which are used in our simulations. To incorporate the long-range bending effects (those which determine the persistence length of a given polymer), the bending potential energy,  $U_{\text{bend}}$ , is calculated for each pair of bonds. It is more favorable to have a configuration with a lower energy. This total potential energy is given by

$$\frac{U_{\text{bend}}}{k_B T} = \beta U_{\text{bend}} = \kappa \sum_{j=1}^{N-1} (1 - \cos \theta_j), \quad (5)$$

where  $\beta$  is defined as the reciprocal of the product of the temperature and the Boltzmann constant (an often used scaling factor for molecular energies) and  $\theta_j$  is the angle between bonds labeled  $j$  and  $j + 1$ . The bending constant,  $\kappa$ , is related to the Kuhn length,  $b$ ,

through<sup>27</sup>

$$\frac{b}{a} = \frac{\kappa - 1 + \kappa \coth \kappa}{\kappa + 1 - \kappa \coth \kappa}. \quad (6)$$

In one limiting case,  $\kappa \rightarrow 0$ , there is no bending energy, so the Kuhn length is equivalent to the width of each bead and the system acts as a freely-jointed chain. In cases where the system acts like a WLC, the persistence length is related to the Kuhn length via

$$l_p \equiv \frac{b}{2}. \quad (7)$$

The other source of potential energy in this model comes from the excluded volume of each discretized sphere in the polymer chain. The excluded volume is defined as infinite in the case where two beads are intersecting each other, and zero elsewhere. If a configuration's energy ever goes to infinity, it is no longer a valid configuration and will be rejected. The definition of this energy for every pair of beads  $i$  and  $j$  is given as

$$\frac{U_{\text{EV}}}{k_B T} = \beta U_{\text{EV}} = \begin{cases} \infty & |r_{ij}| \leq w \\ 0 & |r_{ij}| > w \end{cases}, \quad (8)$$

where  $|r_{ij}|$  is the distance between the bead centers. In most of our cases,  $w = a$ , which means the chain will appear as a sequence of touching beads. This gives another method of calculating the contour length of these chains,

$$L = Na = Nw. \quad (9)$$

## 2.5 Pruned-Enriched Rosenbluth Method

There are many advantages of the Pruned-Enriched Rosenbluth Method (PERM) over the previously mentioned polymer simulation methods. Random walks of ideal chains will typically produce Gaussian distributions of the end-to-end distance, whereas PERM is able

to sample over the entire space, including rare events.<sup>28</sup> While the self-avoiding walks will either give short chains or rejects collisions outright, PERM always returns simulations of the desired length. The simulation code used to produce these data was developed internally by Douglas Tree and Abhiram Muralidhar within the Dorfman Group using the DWLC model and the PERM for building polymer chains.

The Rosenbluth method of sampling<sup>29</sup> is based on the self-avoiding walk algorithm, but adds a bit of intelligence to it. With a self-avoiding walk, the algorithm will reject a configuration as soon as it tries to put the next monomer in an already occupied location, which tends to generate very short chains. In simulating DNA, for example, it is necessary to simulate long chains to replicate the long-range bending properties seen in experimental trials. ( $\lambda$ -DNA, a standard DNA molecule used experimentally, is 48502 base pairs in length.<sup>30</sup>) To overcome this length restriction, Rosenbluth sampling makes an educated guess as to where the next monomer will be placed. The information that the algorithm uses is referred to as the *atmosphere*, which is the number of ways that a certain configuration can add another monomer.<sup>28</sup> On a lattice, the atmosphere,  $a$ , is well defined: for a one-dimensional ideal random walk,  $a = 2$  since it can always go in the positive direction or in the negative; for a two-dimensional ideal random walk,  $a = 4$  for the positive and negative directions of each dimension. Self-avoiding walks pose a more complicated problem, since the first point has an atmosphere of  $a_1 = 4$  to place the second point, but  $a_2$  (to place the third point) immediately decreases to 3 since it cannot return to the location of the first monomer. (The first point is placed with “infinite” atmosphere, hence  $a_0$  is ignored.) As the self-avoiding walk continues on this two-dimensional square lattice,

$$a_i \in \{3, 2, 1, 0\} \text{ for } i > 1, \tag{10}$$

depending on the configuration of already-placed monomers. In the unfortunate case where  $a_i = 0$ , the configuration is trapped and cannot add the next monomer, and is therefore not

able to reach the desired length, commonly known as attrition.<sup>31</sup> This is similar to the self-avoiding walk algorithm since many trial configurations will be terminated early, drastically reducing the number of full-length configurations returned.

The atmosphere of a certain configuration defines the number of possible directions that a chain can continue growing, but only one direction will be chosen with a probability of

$$p_i = \frac{1}{a_i} \quad (11)$$

at each point  $i < N$ , if there is no other energy acting upon the chain. Since each point  $i$  will have a different atmosphere, this probability will induce a bias because some chains will have no choices where to go ( $a_i = 1$  for some time), whereas others will grow through relatively open space. To correct for this, Rosenbluth sampling<sup>28</sup> corrects this by giving each generated chain a weight,

$$W_n = \prod_{i=0}^{n-1} a_i, \quad (12)$$

which occurs with an overall probability of

$$P_n = \prod_{i=0}^{n-1} p_i = \prod_{i=0}^{n-1} \frac{1}{a_i}, \quad (13)$$

giving  $P_n W_n = 1$ , thereby removing any bias obtained from the introduction of the atmosphere. This weight is then used in calculating statistical properties, such as the average extension and average radius of gyration.

As previously mentioned, Rosenbluth sampling alone cannot remove the attrition of long chain samples completely (but it does greatly improve over self-avoiding walks). Grassberger<sup>32</sup> developed pruning and enriching strategies to aid Rosenbluth sampling in order to produce long chains with approximately no attrition. There are several techniques proposed by Grassberger<sup>32</sup> and later by Janse van Rensburg,<sup>33</sup> which are quite complex. Essentially, the algorithm will grow a tree of chains (a tour) that will be *enriched* by gaining branches if

the atmosphere is relatively large or be *pruned* by removing a branch with a relatively low atmosphere.

In our case, calculating the atmosphere is quite difficult because the simulation is not restricted to a lattice and has a weighted distribution of trial points based on potential energy. Since our algorithm<sup>26</sup> is not restricted to a lattice, there are an infinite number of possible directions for the next monomer to be placed, which would generate infinite atmosphere for every step. Thus, a parameter must be passed to our algorithm that determines how many trial points to test; we commonly use an atmosphere of  $K = 5$  trial points. When the algorithm is choosing which atmospheric points to try, it uses the bending potential energy (equation 5) to determine the probability distribution of directions. To calculate the weight of each trial point, we factor in the excluded volume potential energy (equation 8) at each  $n^{\text{th}}$  step via<sup>26</sup>

$$a_n^{(k)} = \exp(-\beta U_{EV,n}^{(k)}). \quad (14)$$

One of these trial steps will be randomly chosen using the probability

$$p_n^{(k)} = \frac{a_i^{(k)}}{w_n}, \quad (15)$$

where  $w_n$  is the overall weight of the  $n^{\text{th}}$  growth step given by

$$w_n = \sum_{k=1}^K a_n^{(k)}. \quad (16)$$

The weight of the entire polymer configuration is multiplicative to give an  $n^{\text{th}}$ -step weight of

$$W_n = \prod_{i=0}^n w_i. \quad (17)$$

The pruning/enriching parameter is the weight of the chain compared to its ensemble average weight,  $\langle W_n \rangle$ . When the specific weight of a chain is lower than the ensemble average, the chain is running out of open spaces in which to grow, meaning it is not a



favorable branch and is pruned. In the other case where the weight is much higher than the average, the algorithm will create branches from this point in the chain.<sup>26</sup> A downside to these enrichments is that many tours may share parts of their configurations because a long chain could enrich at the last bead, producing two chains that differ only in the last bead. Due to this, the algorithm is set up to generate many tours, but only write a small percentage (1–5 %) to the data files. This is to remove the bias of very similar chains. When the algorithm has made its  $N^{\text{th}}$  step, it is finished and the chain is the desired length.  $W_N$  can then be used in calculating the weighted statistical properties for chains of length  $N$  or as a function of chain length.

Other improvements made to our specific algorithm by Douglas Tree and Abhiram Muralidhar include making educated predictions and parallelizing the computation scheme. It is difficult to estimate the ensemble weight average for a set of parameters before running any simulations. To generate a rough value, the code first runs a “blind” simulation to estimate  $\langle W_n \rangle$ , which it then can extrapolate to long chains:<sup>26</sup> at large  $n$ ,

$$\log \langle W_n \rangle \propto n. \tag{18}$$

The code starts with a blind simulation of a small chain of 51 beads (50 segments) to give an estimate of  $\langle W_n \rangle$ , and then repeats with a “non-blind” simulation, using the estimated  $\langle W_n \rangle$  as the pruning/enriching parameter. Then, it approximately doubles the number of segments and repeats the process. When the desired chain length is almost reached, the simulation performs a “full” run-through, generating the final configuration that is saved as the simulation’s output. During this full simulation, properties such as the span and end-to-end distance are calculated on the fly, depending on what flags the user has set.

The full simulation runs in Fortran 90 on a Dell Linux cluster at the Minnesota Supercomputing Institute, using a master/slave scheme to fully utilize its parallel computing abilities.

## 3 Theories

### 3.1 Global Persistence Length

While the standard persistence length of a polymer,  $\ell_p$ , describes the local bending properties, there are larger-scale attributes that cannot be accurately predicted with only the persistence length. A so-called *global* persistence length was proposed<sup>6</sup> for worm-like chains near the classic Odijk regime<sup>2</sup> to better explain these long-range conformational shapes. In strong confinement, the channel size is not large enough to allow for the chain to change direction, or backfold. However, as we transition into slightly larger channels, we observe backfolding.

From a visual standpoint, the global persistence length defines the distance along a channel between two hairpin turns, which are approximately where the polymer changes direction along the channel's main axis. In vector geometry terminology, a hairpin turn is where the polymer chain's turning angle<sup>25</sup> to the channel's main axis reaches  $\pm 90^\circ$ . With a large enough sample size (either in number of simulations and/or length of chains), finding the mean distance between hairpin turns might be feasible, but is not useful for smaller samples.

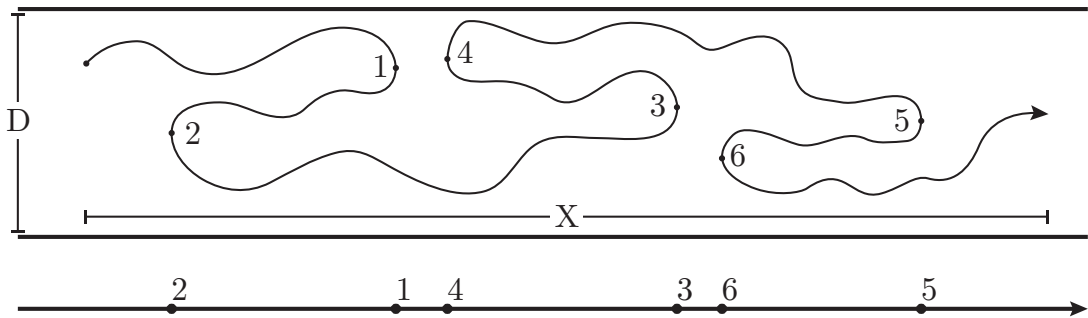


Figure 6: A continuous WLC model in two dimensions exhibiting hairpin backfolding under near-strong confinement. The channel size is  $D$  and the extension along the channel is labeled with  $X$ , equivalent in this case to the end-to-end distance along the channel axis,  $R_x$ . The global persistence length,  $g$ , is the average distance between two consecutive hairpins (labeled 1 - 6) when projected onto the axis along the channel, shown beneath the visual representation of the polymer.

For individual samples, a more helpful method of determining the global persistence length is to fit a function relating the projection of the mean square end-to-end distance,  $R_x^2$  onto the main channel axis to the contour length<sup>4</sup> via

$$R_x^2 = \frac{1}{3} (1 + 2m) [2gL - 2g^2 (1 - \exp(-L/g))], \quad (19)$$

where  $m$  is an orientational order parameter<sup>34</sup> of the average of the second Legendre polynomial of  $\cos \theta$ ,

$$m \equiv \langle P_2(\cos \theta) \rangle = \left\langle \frac{3 \cos^2 \theta - 1}{2} \right\rangle. \quad (20)$$

At the limit of large  $L$ , the long chain limit, the exponential term drops out, giving a simple polynomial in  $g$ . In fact, if we plot  $R_x^2/L\ell_p$  versus  $L/\ell_p$ , equation 19 transforms into a dimensionless form,

$$\frac{R_x^2}{L\ell_p} = \frac{1 + 2m}{3} \left[ 2 \left( \frac{g}{\ell_p} \right) - 2 \left( \frac{g}{\ell_p} \right)^2 \left( \frac{\ell_p}{L} \right) \left( 1 - \exp \left( -\frac{L}{\ell_p} \cdot \frac{\ell_p}{g} \right) \right) \right], \quad (21)$$

which, at  $L/\ell_p \rightarrow \infty$ , further reduces to

$$\frac{R_x^2}{L\ell_p} = \frac{2(1 + 2m)}{3} \left( \frac{g}{\ell_p} \right). \quad (22)$$

This implies that if we have long chains with enough samples to calculate  $m$  adequately, the global persistence length can be found directly from the limit of equation 22. Hence, the value of the horizontal asymptote of the plot of  $R_x^2/L\ell_p$  versus  $L/\ell_p$  is sufficient to obtain a value of the global persistence length.

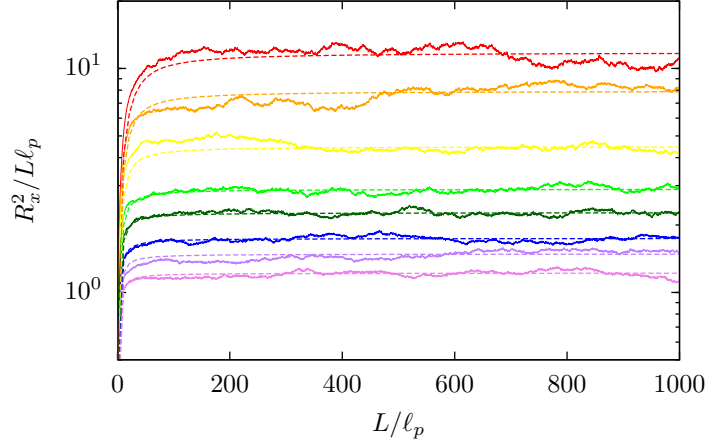


Figure 7: An example plot of 8 worm-like chain simulations of the same persistence length in differently-sized channels fitted with a dotted line to find  $g$ . Each simulation reaches a horizontal asymptote before  $L/\ell_p = 200$ , which was the cutoff point for fitting these curves in the asymptotic region. These simulations shown here have one dimension held at  $D/\ell_p = 1$ , while the other dimension varied such that  $D/\ell_p = \{0.5, 0.75, 1, 2, 3, 5, 10\}$ , from top to bottom, respectively.

The trend of global persistence length as a function of channel size has been studied in both theoretical and computational capacities. The simulation result<sup>4</sup> did not line up with the theory<sup>6</sup> in its original form, but was off by a prefactor. Since a real polymer may not be perfectly oriented along a nanochannel, the global persistence length may be smaller than expected for polymers that are not well-oriented. This prefactor was able to be explained by an extra force inherent in the fluctuations within the hairpin curve shape,<sup>4,34</sup> since Odijk<sup>6</sup> did not account for these fluctuations.

The general equation<sup>6</sup> for the global persistence length as a function of channel size (for square channels) is

$$\frac{g}{\ell_p} = \alpha \left( \frac{\ell_p}{\bar{r}} \right) \exp \left( \frac{\bar{F}}{k_B T} \right), \quad (23)$$

which Odijk found  $\alpha = 3.3082$  through numerical integration. The average length of a hairpin chord,  $\bar{r}$ , is given by

$$\frac{\bar{r}}{\ell_p} = \frac{1}{6} \left( \sqrt{E_m^2 + 6\sqrt{2}E_m \left( \frac{D}{\ell_p} \right)} - E_m \right), \quad (24)$$

with  $E_m = 1.5071$  found through another numerical integration of Odijk’s model. The force on the polymer hairpin,  $\bar{F}$ , is then

$$\frac{\bar{F}}{k_B T} = E_m \left( \frac{\ell_p}{\bar{r}} \right) - 3 \ln \left( \frac{D - \bar{r}\sqrt{2}}{D} \right) - \ln \left( \frac{8}{3\pi} \right) \quad (25)$$

and fit simulation data for square channels with great accuracy.<sup>4</sup> This theoretical relation has not yet been extended to channels of rectangular cross-section. Furthermore, this relation is only valid in the limit of strong confinement, so it cannot be used with great confidence for  $D > \ell_p$ . This strict cutoff point is defined by the model through Odijk’s numerical integrations and data fitting, unlike other regime cutoff points that are rough estimations. At large channel sizes, the global and local persistence lengths collapse,<sup>4</sup> due to extremely weak confinement, validating the name of global *persistence length*.

### 3.2 Odijk Scaling Theory

Under the right conditions, a confined polymer can form hairpins or exhibit backfolding. A new regime was posited by Odijk<sup>6</sup> as distinct from the traditional regimes of de Gennes<sup>3</sup> and Odijk,<sup>2</sup> as well as the “extended de Gennes” regime.<sup>5</sup> To obtain general predictions for a polymer’s extension during backfolding within a nanochannel, Odijk<sup>7</sup> introduced a dimensionless scaling parameter,  $\xi$ , that allowed him to collapse many different situations into a general scaling relation. In the conditions specified by Odijk,<sup>7</sup> the general relation between average extension along the channel direction of a polymer chain,  $\langle X \rangle$ , to its scaling parameter is given by

$$\langle X \rangle \simeq L \xi^{1/3}, \quad (26)$$

where  $L$  is the contour length, which corresponds to the more commonly reported fractional extension scaling relation of

$$\frac{\langle X \rangle}{L} \simeq \xi^{1/3}. \quad (27)$$

This is only valid in the regime where  $\xi < 1$ . As  $\xi \rightarrow 1$ , the magnitudes of  $\langle X \rangle$  and  $L$  become very similar. Since equation 27 is not a strict equality, the ratio of the two cannot be definitively stated;  $\xi = 1$  does not necessarily imply that  $\langle X \rangle = L$ . In the regime where  $\xi > 1$ , there will be a crossover point where  $\langle X \rangle > L$  in this model. The contour length is defined as the distance along the backbone of the polymer, regardless of bends or folds, whereas the extension is the overall distance from one side of a polymer coil to the other, along the direction of the nanochannel. With these physical definitions, if  $\langle X \rangle = L$ , this implies that the polymer is completely straight and aligned to the channel's axis. To attempt to increase the extension without affecting the contour length, this completely straight polymer must then be *further* stretched, which will only lead to breaking of the chain, leading to the breakdown of Odijk's backfolding scaling relation.

To differentiate the distinct cases presented by Odijk,<sup>6</sup> he defines  $\xi_1$ ,  $\xi_2$ ,  $\xi_3$ , and  $\xi_4$  as different scaling parameters for different regimes. The first two are for square nanochannels, while the latter two are for rectangular nanochannels. (Odijk calls them “nanoslits”.) They are presented in terms of raw variables as well as their dimensionless equivalents. The first case is for square nanochannels with strong confinement ( $D \ll \ell_p \ll L$ ), where the scaling parameter is defined<sup>7</sup> by

$$\xi_1 = \frac{gw}{D^{5/3}\ell_p^{1/3}} = \left(\frac{g}{\ell_p}\right) \left(\frac{D}{\ell_p}\right)^{-\frac{5}{3}} \left(\frac{\ell_p}{w}\right)^{-1}, \quad (28)$$

which has been previously verified<sup>4</sup> by simulations similar to those presented in this publication. The second case is valid for large channels ( $D \gtrsim \ell_p$ ) within the “blob” regime, with the scaling parameter defined<sup>7</sup> as

$$\xi_2 = \frac{\ell_p w}{D^2} = \left(\frac{D}{\ell_p}\right)^{-2} \left(\frac{\ell_p}{w}\right)^{-1}. \quad (29)$$

Since this regime requires large channels, which requires long chains (many beads), it does not lend itself well to simulations due to the computational time and space required to

perform these simulations being much too large. If the channel size is increased even further to  $D \gg \ell_p$ , the polymer is essentially in its bulk state (unconfined), which is not of interest to these studies.

Now we come to the regime on which this publication is focused. In the case of rectangular nanochannels (or nanoslits), there are now two cross-sectional spatial dimensions; call them  $D_1$  and  $D_2$  such that  $D_2 \geq D_1$ . The third scaling parameter is given<sup>7</sup> by

$$\xi_3 = \frac{gw}{D_2^{2/3} D_1 \ell_p^{1/3}} = \left(\frac{g}{\ell_p}\right) \left(\frac{D_1}{\ell_p}\right)^{-1} \left(\frac{D_2}{\ell_p}\right)^{-\frac{2}{3}} \left(\frac{\ell_p}{w}\right)^{-1}. \quad (30)$$

In the degenerate case where  $D_2 = D_1$ , equation 30 becomes equation 28. In section 4.2, we present simulation results that support Odijk's third scaling relation.

The final scaling parameter is useful in a regime of rectangular nanochannels where  $D_2 \gtrsim \ell_p$ , in the “blob” regime. Much like  $\xi_2$ ,  $\xi_4$  requires nanochannels that are large in at least one dimension. While simulations for this regime would be more manageable than those required to calculate  $\xi_2$ , they are still somewhat unwieldy to simulate. The relation for Odijk's final scaling parameter<sup>7</sup> is

$$\xi_4 = \frac{\ell_p w}{D_2 D_1} = \left(\frac{D_1}{\ell_p}\right)^{-1} \left(\frac{D_2}{\ell_p}\right)^{-1} \left(\frac{\ell_p}{w}\right)^{-1}. \quad (31)$$

If  $D_2$  is increased even further, the polymer is essentially confined in only one dimension, giving two-dimensional excluded volume effects.<sup>35</sup> Like with small-channel regimes, the degenerate case of  $D_2 = D_1$  transforms equation 31 into equation 29, verifying the simpler square channel relations.

## 4 Simulation Results

### 4.1 Ideal Chains

In the definition of the global persistence length,<sup>6</sup> it is not subject to the effects of excluded volume. Because of this, we can simplify the simulations required to generate statistics for the global persistence length. The simulation time for ideal chains is drastically lower than that required for real chains (with all other parameters held constant), which can increase the efficiency of research techniques and help determine trends in the data without attempting to perform “real-world” simulations with all interaction effects incorporated. The global persistence lengths calculated can then be used in the equation 30, if the other parameters are the same.

While the general Odijk regime (both classical and backfolded) is valid for  $D \lesssim \ell_p$ , some of the smaller channel sizes cannot be reasonably reached with our simulations, since the global persistence increases exponentially with decreasing channel size.<sup>4</sup> This means that the simulations will require exponentially longer chains in order to observe an adequate number of hairpin turns. To avoid these extremely long chains, we will limit the channel size to  $D_1, D_2 \geq 0.5\ell_p$ , which will still allow a wide range of channel sizes to be simulated. Depending on the aspect ratio of the cross-sectional dimensions of the channel, we may be able to use  $D_1 < \ell_p$  as long as  $D_2 \gg \ell_p$ , to give the chain enough cross-sectional area to be able to backfold. Nevertheless, for simplicity, the simulations are restricted to the more well-defined minimum dimension of  $0.5\ell_p$ .

The space that the simulations with cover is defined by the persistence length, the aspect ratio and the channel dimensions. An arbitrary upper limit of  $D_1, D_2 \leq 20\ell_p$  was used, which allows for the observation of asymptotic behavior of  $g/\ell_p \rightarrow 1$  at larger channel sizes. The results for these simulations are shown in figure 8.



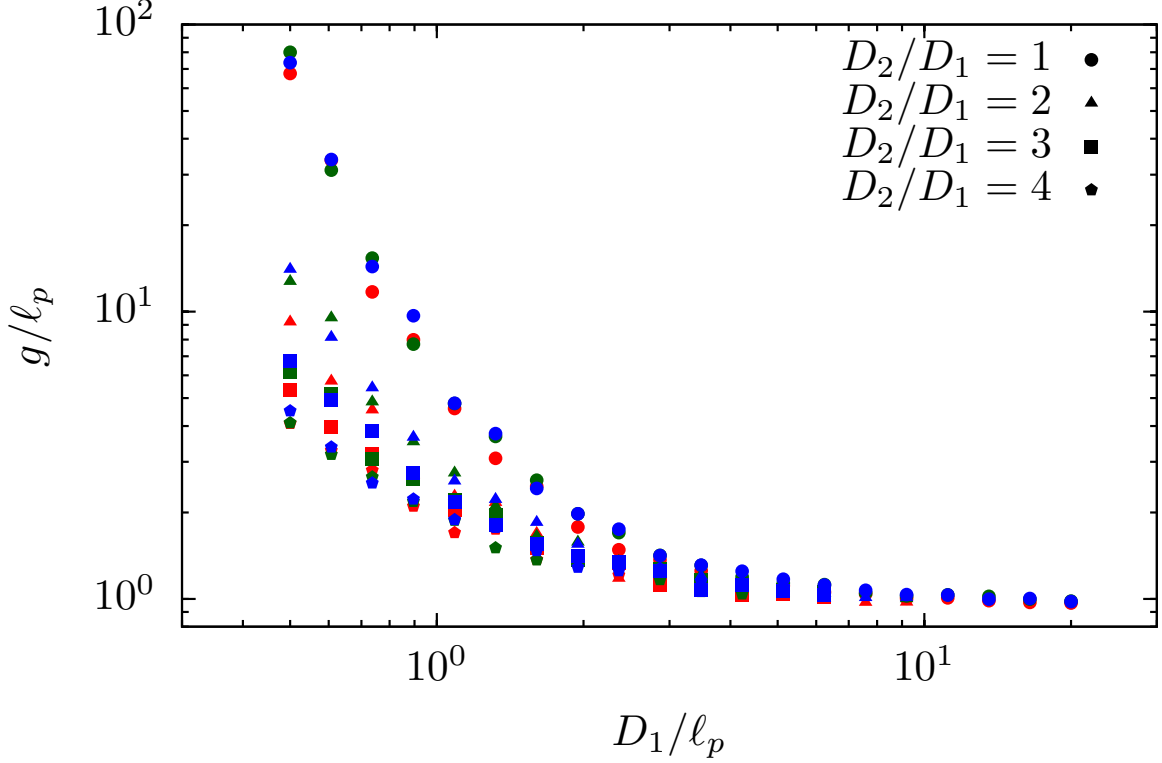


Figure 8: A plot of global persistence length versus the shorter channel dimension for 4 different aspect ratios. Within each data set are 3 persistence lengths of  $\ell_p/w \in \{10 \text{ (red)}, 15 \text{ (green)}, 20 \text{ (blue)}\}$ , which do not show any trends between each other. The asymptotic limit of  $g/\ell_p \rightarrow 1$  in weak confinement demonstrates the collapse of the global and local persistence length. (The values do dip below  $g/\ell_p = 1$ , but can be explained due to statistical fluctuations in the global persistence length.)

The general shape of these trends mimics the form described by theory<sup>6</sup> as well as by demonstrated by simulations.<sup>4</sup> The prefactor, however, is not consistent between the various aspect ratios represented in figure 8. There is no theory yet to describe the difference in trends of global persistence length versus channel size for different aspect ratios of rectangular cross-section. It is well expected<sup>4</sup> that the global persistence length degenerates into the standard persistence length at large channels (weak confinement), but the interesting fact is that the different aspect ratios seem to reach the asymptotic limit at the same approximate channel size. This may be due to the lack of a wide range of aspect ratios; a different trend may be observed for larger aspect ratios.

## 4.2 Real Chains

While the global persistence length of a chain's configuration can be calculated using ideal (no excluded volume) chains, the extension must be determined by running simulations that incorporate the excluded volume effects into the configurations. To compare the data between ideal and real chains and to use equation 30, the nanochannel's effective dimensions must remain the same. Since the ideal chains have no excluded volume, the center of any bead can be placed right next to the wall of the nanochannel. Meaning the effective dimensions are

$$D_{1,\text{eff}} \times D_{2,\text{eff}} = D_1 \times D_2. \quad (32)$$

However, when the beads are given a solid volume with a diameter  $w$ , the closest the centers of the beads can be to the wall of the nanochannel is at a distance of  $w/2$  inside the wall. This forbidden area is located along every wall of the channel, reducing each dimension equally by a total of  $2 * w/2 = w$ . Due to this, the effective dimensions the become

$$D_{1,\text{eff}} \times D_{2,\text{eff}} = (D_1 - w) \times (D_2 - w). \quad (33)$$

With these effective channels dimensions and the global persistence lengths generated in the simulations presented in section 4.1, we can then rerun the simulations, this time reincorporating the excluded volume effects. Some of the simulations performed had channel sizes much larger than  $\ell_p$ , which lie outside of the classic Odijk regime. The classic Odijk regime is valid for  $D \lesssim \ell_p$ , which we can loosely define as  $D \leq 2\ell_p$ , as supported by experiment.<sup>36</sup> As a simple extension to rectangular cross-sections, we will use this cutoff size in both dimensions of the rectangular channels. This may drastically reduce the possible channel sizes, but should still allow us to cover relevant values of  $\xi_3$ .

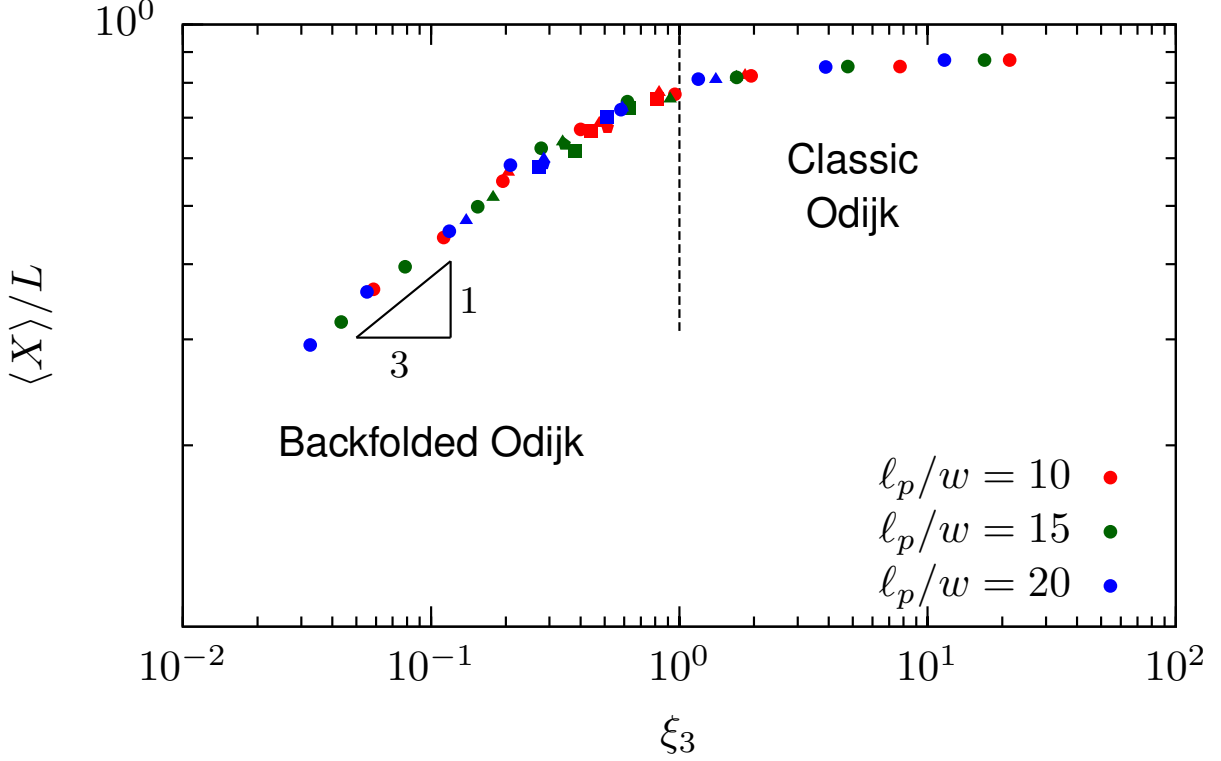


Figure 9: A plot of fractional extension versus the scaling parameter,  $\xi_3$ , for 3 different values of persistence length, scaled by the width of the chain, for real worm-like chain. As predicted,<sup>7</sup> the backfolded Odijk regime breaks down around  $\xi_3 \simeq 1$ . In addition, these data correspond to the same fractional extension as square channels for most values of  $\xi_3$ . The aspect ratios of the rectangular channels shown here are  $D_2/D_1 \in \{1 (\circ), 2 (\triangle), 3 (\square), 4 (\diamond)\}$  for each value of persistence length.

The results of these simulations are plotted in figure 9. The accuracy of Odijk’s definition<sup>7</sup> of  $\xi_3$  is apparent through the collapse of 3 distinct values of dimensionless persistence length onto the same curve. In addition, the backfolding regime is typically valid for  $D_1, D_2 \ll \ell_p$ , but give a sound estimate even at  $D_1, D_2 \approx \ell_p$ . It appears that the data deviate from the scaling law at  $\xi_3 \approx 0.5$ , but not appreciably. The noticeable deviations from the scaling law are near  $\xi_3 \approx 1$ , as predicted.<sup>7</sup> For the simulation parameters specified in this publication, the scaling law stated in equation 27 is supported.

## 5 Summary & Future Work

Based on the simulation results presented here, the proposition of a backfolded Odijk regime<sup>6</sup> for worm-like chains confined to rectangular nanochannels is supported through the agreement of global persistence length versus channel size trends for several aspect ratios and persistence lengths. In addition, these trends (for a constant aspect ratio) collapse when made dimensionless by dividing by the persistence length, much like the behavior of square channels.<sup>4</sup> A scaling theory may allow for the various aspect ratios to collapse onto a single curve, but the correct relation has yet to be proposed.

To support the backfolded Odijk regime, scaling parameters,  $\xi_{1-4}$ , were proposed<sup>7</sup> to characterize the fractional extension of polymers within this regime. The simulation data in this work we able to confirm this scaling relation for rectangular channels, corresponding to  $\xi_3$  in equation 30. In addition, the crossover point of  $\xi_3 \approx 1$  is shown to be a reasonable estimate for the transition between the classic Odijk regime and its backfolded counterpart.

While the initial plot of the fractional extension versus  $\xi_3$  (figure 9) agrees with the scaling relation, there are more calculations required to show that the data generated by our simulations are valid. One of the most important metrics to determine if adequate statistics were reached during the simulation is the variance of the extension,  $\delta X^2$ . In the backfolded Odijk regime, the variance has not been shown to collapse like the more classic regimes. In fact, for different persistence lengths, the chains show a wide range of variance for a small range of channel size.<sup>4</sup> However, with the introduction of Odijk's  $\xi$  parameters, the variance data seem to collapse. If we can replicate these properties for rectangular channels, then Odijk's backfolded regime will be even further verified.

Using similar simulation parameters, extending our data into the more traditional regimes to span the channel size variable could explain the transitions between the four main regimes of polymer confinement, or even reveal a possible micro-regime to further our understanding of polymer dynamics. The difficulty with spanning any dimension is that simulation techniques are typically specific to certain types of situations. For instance, to span all channel

sizes, the simulations presented in this work would require extremely long chains to observe some properties such as global persistence length (on the order of billion- or trillion-bead chains in extreme confinement,  $D \ll \ell_p$ ).

Another method of verifying the backfolded Odijk regime would be through experimental methods. With our simulations, the polymer is built from nothing on the inside of the channel. In experiments, polymers such as DNA are forced into channels, possibly causing biases in their configurations. An interesting, albeit extremely fantastic, way to emulate our simulations in physical space would be to form a polymer *in situ* on the inside of a confinement channel. However, most polymerization schemes will not allow for this, but this might be a direct verification of our simulation methods.

The future work proposed for this research topic within the Dorfman group involve looking into the variance and more simulation parameters to ensure that the backfolding scaling relation is applicable for the entire variable space specified. Varying  $w$ , the width of the beads, will allow for a new set of intrachain interactions, including crossing of bonds without violating the excluded volume potential energy for  $w < 1$ . Since this is taken into account in  $\xi_3$ , these data should collapse as well onto the Odijk scaling law.<sup>7</sup>

## 6 Acknowledgements

The simulation code was initially developed by Douglas R Tree under the supervision of Kevin D Dorfman at the University of Minnesota, with support through a Doctoral Dissertation Fellowship. The code has been optimized and adapted to rectangular nanochannels and is currently maintained by Abhiram Muralidhar under the supervision of Kevin D Dorfman at the University of Minnesota. Computational resources were provided in part by the University of Minnesota Supercomputing Institute.

## References

- <sup>1</sup> Walter Reisner, Keith J Morton, Robert Riehn, Yan Mei Wang, Zhaoning Yu, Michael Rosen, James C Sturm, Stephen Y Chou, Erwin Frey, and Robert H Austin, “Statics and dynamics of single DNA molecules confined in nanochannels”, *Physical Review Letters* **94**(19), pp. 196101 (2005).
- <sup>2</sup> Theo Odijk, “The statistics and dynamics of confined or entangled stiff polymers”, *Macromolecules* **16**(8), pp. 1340–1344 (1983).
- <sup>3</sup> M Daoud and P-G de Gennes, “Statistics of macromolecular solutions trapped in small pores”, *Journal de Physique* **38**(1), pp. 85–93 (1977).
- <sup>4</sup> Abhiram Muralidhar, Douglas R Tree, and Kevin D Dorfman, “Backfolding of wormlike chains confined in nanochannels”, *Macromolecules* **47**(23), pp. 8446–8458 (2014).
- <sup>5</sup> F Brochard-Wyart, T Tanaka, N Borghi, and P-G de Gennes, “Semiflexible polymers confined in soft tubes”, *Langmuir* **21**(9), pp. 4144–4148 (2005).
- <sup>6</sup> Theo Odijk, “DNA confined in nanochannels: Hairpin tightening by entropic depletion”, *The Journal of Chemical Physics* **125**(20), pp. 204904 (2006).
- <sup>7</sup> Theo Odijk, “Scaling theory of DNA confined in nanochannels and nanoslits”, *Physical Review E* **77**(6), pp. 060901 (2008).
- <sup>8</sup> Paul C Hiemenz and Timothy P Lodge, *Polymer Chemistry*, CRC Press 2<sup>nd</sup> edition (2007).
- <sup>9</sup> George Marsaglia et al., “Choosing a point from the surface of a sphere”, *The Annals of Mathematical Statistics* **43**(2), pp. 645–646 (1972).
- <sup>10</sup> Eric W Weisstein, “Sphere point picking, From MathWorld—A Wolfram Web Resource”, <http://mathworld.wolfram.com/SpherePointPicking.html>.

- <sup>11</sup> Werner Kuhn, “Über die Gestalt fadenförmiger Moleküle in Lösungen”, *Kolloid-Zeitschrift* **68**(1), pp. 2–15 (1934).
- <sup>12</sup> M F Sykes, “Self-avoiding walks on the simple cubic lattice”, *The Journal of Chemical Physics* **39**(2), pp. 410–412 (1963).
- <sup>13</sup> Jacob Mazur and Robert J Rubin, “Average span of self-avoiding walks on the simple cubic lattice”, *The Journal of Chemical Physics* **60**(1), pp. 341–342 (1974).
- <sup>14</sup> Hagai Meirovitch and H A Lim, “Computer simulation study of the  $\theta$ -point in three dimensions. I. self-avoiding walks on a simple cubic lattice”, *The Journal of Chemical Physics* **92**(8), pp. 5144–5154 (1990).
- <sup>15</sup> Vladimir Privman, “Study of the  $\theta$  point by enumeration of self-avoiding walks on the triangular lattice”, *Journal of Physics A: Mathematical and General* **19**(16), pp. 3287 (1986).
- <sup>16</sup> J L Martin, M F Sykes, and F T Hioe, “Probability of initial ring closure for self-avoiding walks on the face-centered cubic and triangular lattices”, *The Journal of Chemical Physics* **46**(9), pp. 3478–3481 (1967).
- <sup>17</sup> Philip Mark and Stanley Windwer, “Self-avoiding walks on the tetrahedral lattice”, *The Journal of Chemical Physics* **47**(2), pp. 708–710 (1967).
- <sup>18</sup> C Domb, “On multiple returns in the random-walk problem”, *Mathematical Proceedings of the Cambridge Philosophical Society* **50**(04), pp. 586–591 (1954).
- <sup>19</sup> H L Abbott and D Hanson, “A lattice path problem”, *Ars Combinatoria* **6**, pp. 163–178 (1978).
- <sup>20</sup> Harry Kesten, “On the number of self-avoiding walks”, *Journal of Mathematical Physics* **4**(7), pp. 960–969 (1963).



- <sup>21</sup> Masao Doi, Samuel Frederick Edwards, et al., *The Theory of Polymer Dynamics* volume 222, Clarendon Press Oxford (1986).
- <sup>22</sup> O Kratky and G Porod, “Röntgenuntersuchung gelöster Fadenmoleküle”, *Recueil des Travaux Chimiques des Pays-Bas* **68**(12), pp. 1106–1122 (1949).
- <sup>23</sup> Nataša Vučemić-Alagić, “Kratky-Porod model”, <http://www-fl.ijs.si/~rudi/sola/KratkyPorodmodel.pdf> (2013).
- <sup>24</sup> C Bouchiat, M D Wang, J-F Allemand, T Strick, S M Block, and V Croquette, “Estimating the persistence length of a worm-like chain molecule from force-extension measurements”, *Biophysical Journal* **76**(1), pp. 409–413 (1999).
- <sup>25</sup> John McCleary, *Geometry from a Differentiable Viewpoint*, Cambridge University Press 2<sup>nd</sup> edition (2012).
- <sup>26</sup> Douglas R Tree, Abhiram Muralidhar, Patrick S Doyle, and Kevin D Dorfman, “Is DNA a good model polymer?”, *Macromolecules* **46**(20), pp. 8369–8382 (2013).
- <sup>27</sup> John A Schellman, “Flexibility of DNA”, *Biopolymers* **13**(1), pp. 217–226 (1974).
- <sup>28</sup> Thomas Prellberg, “From Rosenbluth sampling to PERM – rare event sampling with stochastic growth algorithms”, In R Leidl and A K Hartmann, editors, *Lecture Notes from the 4th International Oldenburg Summer School* volume 12 of *Modern Computational Science* , pp. 311–334. BIS-Verlag der Carl von Ossietzky Universität Oldenburg (2012).
- <sup>29</sup> Marshall N Rosenbluth and Arianna W Rosenbluth, “Monte Carlo calculation of the average extension of molecular chains”, *The Journal of Chemical Physics* **23**(2), pp. 356–359 (1955).
- <sup>30</sup> Donna L Daniels, John L Schroeder, Wacław Szybalski, Fred Sanger, Alan R Coulson, Guo F Hong, Diane F Hill, George B Petersen, and Frederick R Blattner, “Appendix II

- complete annotated lambda sequence”, *Cold Spring Harbor Monograph Archive* **13**, pp. 519–676 (1983).
- <sup>31</sup> Stanley Windwer, “Monte Carlo generation of a restricted random walk and the excluded-volume problem”, *The Journal of Chemical Physics* **43**(1), pp. 115–118 (1965).
- <sup>32</sup> Peter Grassberger, “Pruned-enriched Rosenbluth method: Simulations of  $\theta$  polymers of chain length up to 1 000 000”, *Physical Review E* **56**(3), pp. 3682 (1997).
- <sup>33</sup> E J Janse van Rensburg, “Monte Carlo methods for the self-avoiding walk”, *Journal of Physics A: Mathematical and Theoretical* **42**(32), pp. 323001 (2009).
- <sup>34</sup> Jeff Z Y Chen, “Free energy and extension of a wormlike chain in tube confinement”, *Macromolecules* **46**(24), pp. 9837–9844 (2013).
- <sup>35</sup> P-G de Gennes, “Conformations of polymers attached to an interface”, *Macromolecules* **13**(5), pp. 1069–1075 (1980).
- <sup>36</sup> Liang Dai, Johan van der Maarel, and Patrick S Doyle, “Extended de Gennes regime of DNA confined in a nanochannel”, *Macromolecules* **47**(7), pp. 2445–2450 (2014).